Available online at www.sciencedirect.com
ScienceDirect
Materials Research Bulletin 42 (2007) 113–125
Materials Research Bulletin
www.elsevier.com/locate/matresbu

Microporous titanosilicate AM-2: Rb-exchange and thermal behaviour

Nicola Döbelin *, Thomas Armbruster

Laboratorium für chemische und mineralogische Kristallographie, Universität Bern, Freiestrasse 3, CH-3012 Bern, Switzerland

Received 6 December 2005; received in revised form 11 May 2006; accepted 12 May 2006
Available online 6 June 2006

Abstract

Rb-exchange and thermal stability of the microporous titanosilicate AM-2 were analysed by powder X-ray diffraction, thermogravimetric analysis, and chemical analysis of the mother liquid after exchange. The dehydration and thermal stability of the exchanged structure were monitored with in situ high temperature powder X-ray diffraction. Crystal structures were refined with Rietveld methods at 25 and 400 °C. The AM-2 structure was found to incorporate Rb^+ by replacing K^+. After four exchange cycles and 166 h reaction time at 90 °C, the chemical composition was refined to $K_{0.18}Rb_{1.82}TiSi_3O_9{\cdot}H_2O$. Extrapolation suggests that higher exchange ratios may be obtained after further cycles. H_2O was expelled by heating, leading to a dehydrated structure at 360 °C. Dehydration was associated with a change of space group symmetry from orthorhombic $P2_12_12_1$ to monoclinic $P2_1$, which proved to be reversible after rehydration. This change of symmetry leaves the AM-2 characteristic structural topology uninfluenced and causes only minor distortions. The monoclinic AM-2 structure breaks down above 600 °C to become X-ray amorphous, and at 750 °C a wadeite-type phase ($K_xRb_{2-x}TiSi_3O_9$) crystallises. This transformation is irreversible and leads to immobilisation of Rb^+.

Keywords: A. Inorganic compounds; B. Chemical synthesis; C. X-ray diffraction; D. Crystal structure

1. Introduction

Microporous titanosilicates have attracted great attention among mineralogists and material scientists during the last decades. Their versatility in terms of chemical composition, structural features and ion-exchange capabilities makes them interesting candidates for various technical applications, reaching from the treatment of wastewaters [1], to agricultural applications, and to opto-electronic high-tech components [2], just to name a few. With proceeding exploration of new structures, new variations of known phases and new applications, the demand for researchers systematically investigating these materials rises. Although chemical variations have often only marginal influence on the structural topology, they may change the selectivity for certain cation species or the preference for one element over others. In addition the stability under certain pT conditions strongly depends on the exact chemical composition [3]. Systematic investigation of the physico-chemical properties is therefore crucial for optimising existing techniques, as well as for the development of new fields of application.

* Corresponding author. Tel.: +41 32 644 19 87; fax: +41 32 644 11 76.
E-mail address: nicola@doebelin.org (N. Döbelin).

0025-5408/$ – see front matter © 2006 Elsevier Ltd. All rights reserved.
doi:10.1016/j.materresbull.2006.05.006

AM-2 ($K_2TiSi_3O_9 \cdot H_2O$) [4] is a synthetic analogue of the rare natural zirconosilicate umbite ($K_2(Zr_{0.69}Ti_{0.31})Si_3O_9 \cdot H_2O$) that was found in the Khibiny alkaline massif on Kola peninsula, Russia [5]. Since the discovery of AM-2 many studies describing its synthesis with different chemical compositions have been published [6], the ion-exchange behaviour has been analysed [3,7,8], and the structure has been refined from single-crystal X-ray diffraction data [9].

The structure of AM-2 is made up of a framework of TiO_6 octahedra and SiO_4 tetrahedra (Fig. 1). There are no direct Ti–O–Ti connections, but alternating …–O–Ti–O–Si–… chains along *a*, *b*, [1 0 1] and [1 0 −1]. A one-dimensional open channel system is running along *c* consisting of eight-membered rings of approximately 6 Å × 8 Å in diameter, measured from centres of O sites. These continuous channels are interconnected by a set of non-continuous tubes composed of seven- and eight-membered rings in the (0 0 1) plane (Fig. 2). The polyhedral

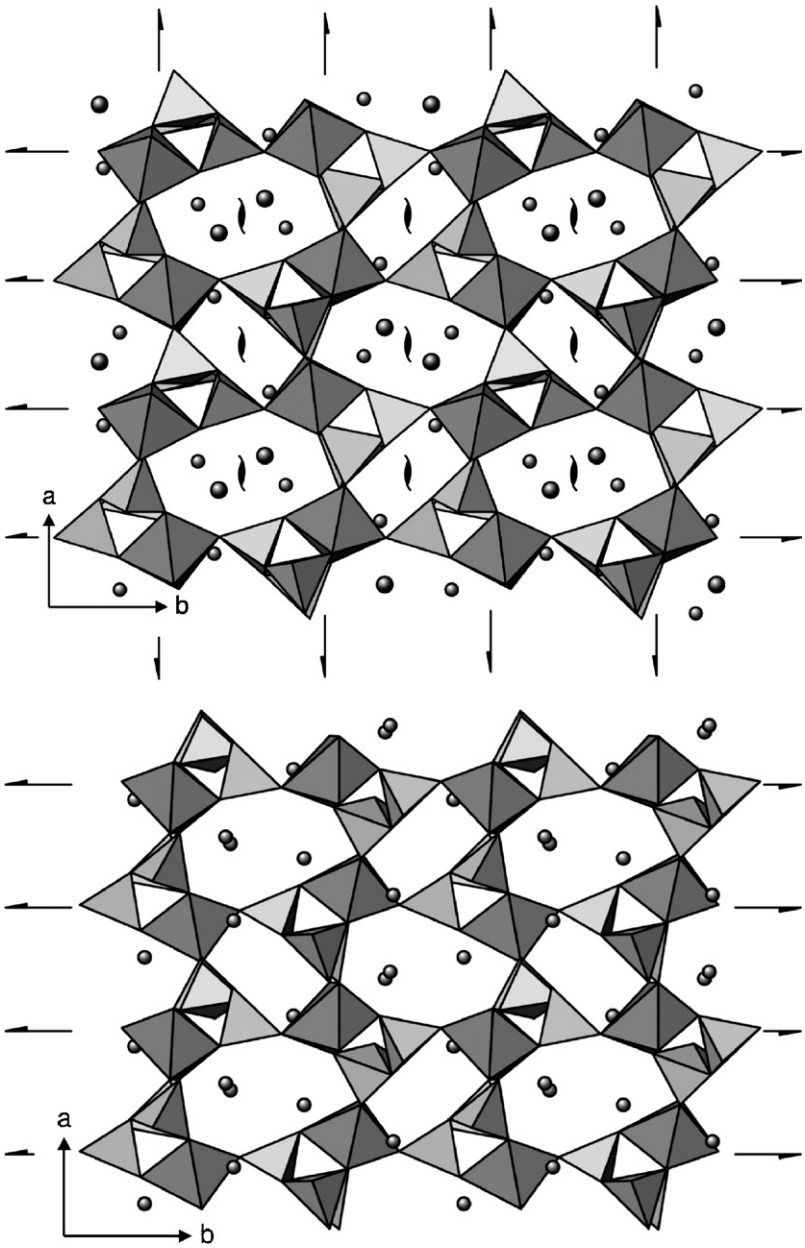

Fig. 1. The two phases of Rb-exchanged AM-2 at 25 (top: fully hydrated, orthorhombic $P2_12_12_1$) and 400 °C (bottom: dehydrated, monoclinic $P2_1$). Small spheres are cations (Rb, K), large spheres represent H_2O molecules. Notice the 2_1 screw axis in the centre of the large channels of the hydrated phase, which is lost upon dehydration. Half-barbed arrows indicate positions of the 2_1 axis within the projection plane.

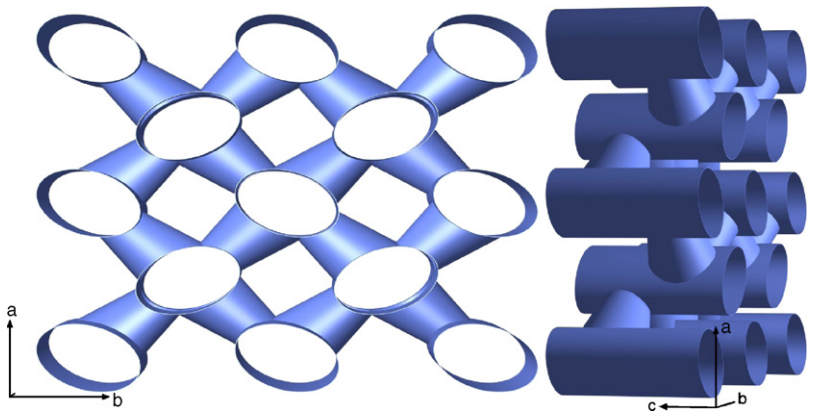

Fig. 2. The channel system of AM-2 shows continuous channels running along *c*. These main channels are interconnected by seven- and eight-membered rings allowing relatively free migration of channel occupants among the tubes.

framework has a negative charge of $2e^-$ per formula unit (pfu), which is compensated by the incorporation of cations into the channel system. Under ambient conditions one H_2O molecule is present.

The aim of the present study is to describe the hydrothermal synthesis of AM-2 of composition $K_2TiSi_3O_9{\cdot}H_2O$ and the ion-exchange of K for Rb. By refining the exchanged structure from powder X-ray diffraction data collected at high temperatures, we provide a detailed analysis of the dehydration behaviour and the thermal stability of Rb-exchanged AM-2.

2. Experimental

Synthesis of AM-2 in this study is based on instructions published in [9] with further optimisations [10]. A mixture of 9.89 g KOH, 4.00 g colloidal SiO_2 (Ludox HS-40), and 2.78 g KCl was added to 29.4 g H_2O and stirred until all solid material was dissolved. 17.96 g $TiCl_3$ solution (15% in 5–10% HCl) were added dropwise. The blackish gel was stirred thoroughly until it was homogeneous and was subsequently filled into Teflon-lined stainless-steel autoclaves. The synthesis was carried out at 200 °C for 5 days in a furnace equipped with a rotating device. The autoclaves revolved at about 3 rounds per minute during the reaction in order to cause agitation. The resulting white powder was washed with H_2O and acetone and dried for 15 min at 50 °C. Powder XRD analysis showed well-crystallised and pure AM-2 without impurities within the detection limit. The material formed aggregates of up to 10 μm in diameter, composed of platy crystallites with lengths of several micro-metres, but sub-micron plate thickness (Fig. 3).

A 1 M exchange solution was prepared by mixing 24.184 g RbCl and 200 ml deionised H_2O. Subsequently 0.4024 g AM-2 of composition $K_2TiSi_3O_9{\cdot}H_2O$ were mixed with 20 ml exchange solution and heated to 90 °C at ambient pressure in a covered Teflon beaker (without stirring). In order to renew the solution the AM-2 powder was filtered off, washed with water and acetone and dried for 15 min at 50 °C. The used solution was kept for further analysis, and the remaining powder was again mixed with 20 ml of fresh solution. The progress of the exchange process was monitored by quantitative analysis of the K^+ concentration in the exchange solution using Inductively Coupled Plasma Optical Emission Spectrometry (ICP-OES).

The dehydration process and total weight loss between 25 and 400 °C were measured by thermogravimetry (TGA) in N_2 atmosphere with a heating rate of 5 °C min^{-1}.

The influence of the dehydration process on the crystal structure was monitored by powder X-ray diffraction with a Philips X'Pert Pro powder diffractometer in Bragg-Brentano theta-2theta configuration. The device was equipped with an Anton Paar HTK-1200 heating chamber, which allows in situ data acquisition from room temperature up to 1200 °C, at ambient pressure and in natural or controlled atmosphere. The Ni-filtered Cu Kα X-radiation from a fine-focus tube lead to a maximum resolution of 1.006 Å at 100° 2θ. Data was collected at 25, 50 °C and further in steps of 50 °C up to 400 °C. The sample was heated at a rate of 5 °C min^{-1} and during data collection the temperature was held constant. After the heating sequence the sample cooled down to 25 °C and a final data set was collected. In a second heating cycle data was collected at 25, 400, 500, 600, 700, and 750 °C, and again after cooling down to room temperature. The experiment was conducted in room atmosphere, moreover the connectors for the atmosphere control

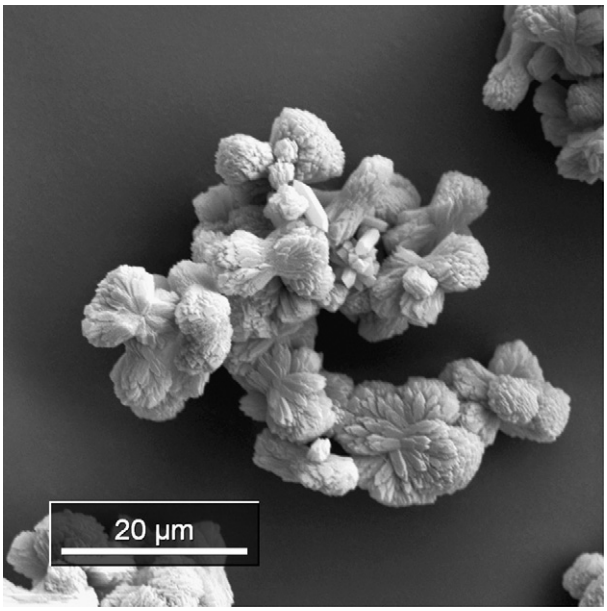

Fig. 3. SEM images of AM-2 show aggregates of up to 10 μm in diameter. The crystallites are platy and less than 1 μm thick. These particles possess a large specific surface allowing fast ion-exchange and dehydration reactions. Furthermore, the risk for orientation effects in powder XRD samples is low due to poor alignment of the crystallites in the aggregates.

system were kept open during the entire procedure in order to allow air circulation. The 25, 400, and 750 °C data sets were recorded from 9 to 100° 2θ and merged from 10 successively recorded measurements in order to obtain maximum resolution and a better signal-to-noise ratio. All other data sets were recorded from 9 to 60° 2θ and used to monitor phase transitions on the basis of unit cell variations. Data sets collected above room temperature were corrected for thermal expansion of the sample stage.

The crystal structures were refined with the software Fullprof [11]. Refinement parameters of the hydrated and dehydrated phase are listed in Table 1. As a starting model for the 25 °C structure the AM-2 structure published in [9] was used. In the first stage of the refinement, only profile parameters such as zeropoint shift, provisional background points and cell parameters were refined in LeBail profile fitting mode. The Thomson-Cox-Hastings pseudo-Voigt function (no. 7 in Fullprof) was used to model reflection profiles. Parameters of the instrument resolution function were determined with a corundum standard sample prior to data collection, and held constant during the entire refinement. After the cell parameters were determined, the model structure was introduced and refined in Rietveld mode with fully occupied Rb on the co-ordinates of the K sites. For the channel occupants a common isotropic

Table 1
Experimental and refinement parameters for Rb-exchanged AM-2

Temperature (°C)	25	400
Space group	$P2_12_12_1$	$P2_1$
a (Å)	10.0851(2)	10.0755(2)
b (Å)	13.0157(2)	12.8625(2)
c (Å)	7.2255(1)	7.1587(1)
β (°)	90	91.754(1)
Cell volume (Å^3)	948.45(3)	927.30(3)
R_{Bragg} (%)	3.48	5.27
R_{p} (%)	8.21	11.5
R_{wp} (%)	7.64	10.6
χ^2	0.39	0.623
No. of variables	62	105
No. of indep. reflections	581	801

displacement parameter was refined. Another isotropic displacement parameter was applied to all remaining framework atoms. The refined framework showed distorted SiO_4 and TiO_6 polyhedra, thus soft distance constraints were applied to all Si–O (1.626(5) Å) and Ti–O bonds (1.962(5) Å). Distances for soft constraints correspond to average Ti–O and Si–O distances obtained from the single-crystal structure published in [9]. In the final step occupancies of Rb sites were refined. After the refinement difference Fourier plots showed remaining electron densities not higher than $\pm 0.4e^-$.

The refined hydrated structure served as starting model for the dehydrated high-temperature structure. The transition from the low-temperature to the high-temperature phase lead to splitting of $h\,0\,l$ peaks in the powder diffraction pattern. The new pattern was indexed in space group $P2_1$, a subgroup of $P2_12_12_1$, with unique b-axis. Due to the lower symmetry all atoms had to be duplicated by the symmetry operation $(x + 1/2, -y + 1/2, -z)$ and shifted by $z + 0.25$ in order to obtain a standard compliant unit cell set-up. The refinement sequence was similar to the hydrated structure including soft distance constraints for framework atoms.

3. Results

As measured by ICP-OES analysis of the exchange solution, a total of 96(5)% of the K^+ ions were exchanged for Rb^+ (Fig. 4). The pH of fresh exchange solution was neutral (7.18), and alkaline after the first exchange cycle (10.25). Alkalinity was less distinct after the following cycles (cycles 2–4: 8.85, 8.08, 7.28), and the stability of Ti-AM-2 was not compromised at any time [7].

The total weight loss measured by TGA amounts to 4.6% of the initial mass. Assuming an ion-exchange ratio of 96% this corresponds to $1.2H_2O$ molecules per formula unit. As shown in Fig. 5, the release of H_2O is steady with a maximum loss rate between 200 and 250 °C, and subsides above 320 °C. Exposed to ambient temperature and humidity (approximately 20 °C and 50% relative humidity in our case) the structure completely rehydrates within a few hours [12].

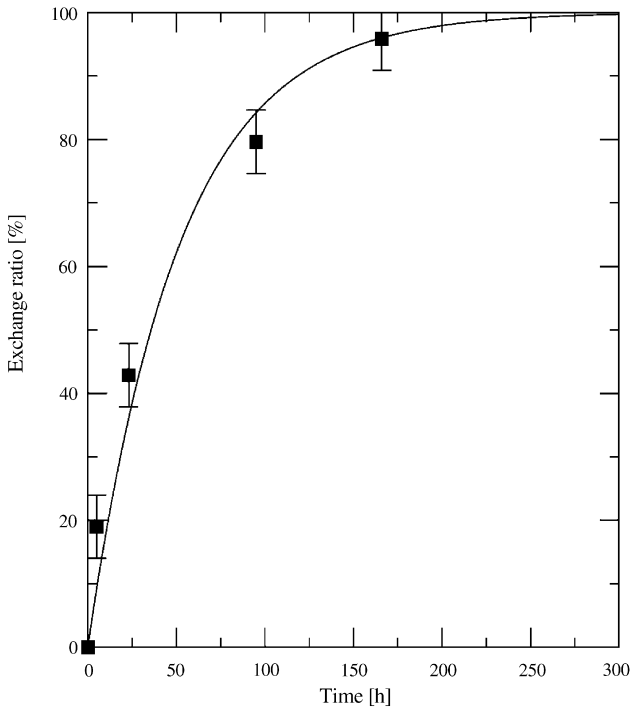

Fig. 4. K^+ concentration in the mother liquid, measured with ICP-OES. The experimental values were fitted with an exponential function $f(x) = -100\exp(-x/51.44) + 100$. According to this function, 99.9% ion-exchange is reached after approximately 355 h. The error bars show a range of ±5%.

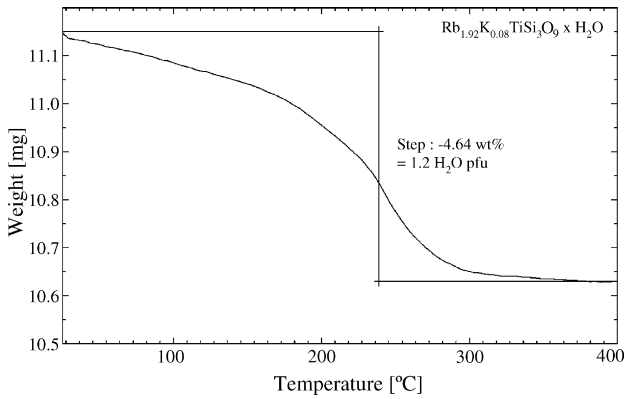

Fig. 5. Dehydration monitored by thermo-gravimetric analysis. The fully hydrated AM-2 structure loses 4.64% of its initial mass when heated from 25 to 400 °C. This corresponds to 1.2H_2O molecules per formula unit.

The hydrated Rb-AM-2 structure shows the same framework structure as K-AM-2 at room temperature, but it has a 3% larger cell volume. The H_2O site Ow1 is located near the centre of a triangle of Rb/K sites in bonding distance to the corners (Ow1–Rb2: 2.63(2), Ow1–Rb1: 2.93(2), Ow1–Rb2: 3.22(2) Å). Two distinct cation positions were found. Since on both sites electron densities were not sufficient for complete Rb occupation, they were refined with scattering factors of both Rb and K, assuming incomplete ion-exchange. The chemical composition was refined to $K_{0.18}Rb_{1.82}TiSi_3O_9{\cdot}H_2O$. Although these cation sites are not solely occupied by Rb, they are herein after referred to as Rb1 and Rb2. For the description of bonding environments a maximum Rb–O bond length of 3.37 Å was assumed, which corresponds to a bond valence of 5% [13]. Very weak reflections of a second AM-2 phase with cell parameters $P2_12_12_1$, $a = 10.008(1)$, $b = 13.012(1)$, and $c = 7.2116(6)$ Å slightly different from the main phase were also observed. The cell parameters of the minor phase lie thus between the initial K-bearing [9] and the Rb-exchanged structure. Reflection intensities were close to the detection limit, hence we estimate the concentration to be <5 wt%. X-ray diffraction patterns of the main phase recorded during heating show a decrease of the unit cell dimensions between 50 and 350 °C (Fig. 6). Between 150 and 200 °C a distinct phase change from orthorhombic to monoclinic symmetry occurs, which coincides with the highest loss rate of H_2O. Complete dehydration is reached at approximately 320 °C. The high-temperature phase remains stable up to 600 °C and completely reverts to the $P2_12_12_1$ low-temperature phase after cooling down to room temperature and rehydration (Table 2). The monoclinic unit cell is slightly smaller than the orthorhombic cell (Tables 1 and 2, Fig. 6); the cell volume decreased by 2.22%, a remained almost constant, and b and c shortened by approximately 1%.

Due to high temperature data collection, high displacement parameters, particularly for weakly bound channel occupants, had to be expected. Thus one common isotropic displacement factor was refined for all channel occupants, and another isotropic displacement parameter was introduced for all framework atoms. To our knowledge the results presented in Table 3 comprise the first structure refinement of this monoclinic high-temperature phase. The topology of the framework is identical to the one of the orthorhombic hydrated phase. Changes are mainly observed in P–O–P angles (P: central atom of polyhedra, O: vertex oxygen), but no rearrangement of polyhedra occurred. Due to the absence of H_2O molecules in the voids, the bonding situations of Rb cations changed slightly. In 0.96(5) Å distance to Rb2b, a new partially occupied site Rb3a was refined. Occupancy factors of these two sites were coupled to a sum of 1.0 and refined to 30% on Rb2b and 70% on Rb3a. The resolution of the experimental data was not sufficient to refine overlapping K and Rb on channel sites, therefore only Rb scattering factors were used, but occupancies <1.0 were allowed on Rb1a, Rb1b, and Rb2a. The sum of electrons on channel-cation sites was refined to 140.86(2), which agrees within two standard deviations with the 139.4(4) e^- found in the orthorhombic structure. The refined composition is thus $Rb_{1.80}K_{0.20}TiSi_3O_9$. The splitting of Rb2 into Rb2b and Rb3a may be an artefact and may also be interpreted as one anisotropically disordered site. This is supported by the high B_{eq} values for channel occupants shown in Table 4. Atomic co-ordinates, occupancy factors and displacement parameters for the hydrated and dehydrated phase are listed in Tables 3 and 4. The dehydrated structure persists up to 600 °C. No increasing amorphous fraction was observed in X-ray diffraction patterns. Between 600 and 700 °C the crystal structure completely breaks down and at 700 °C the material becomes

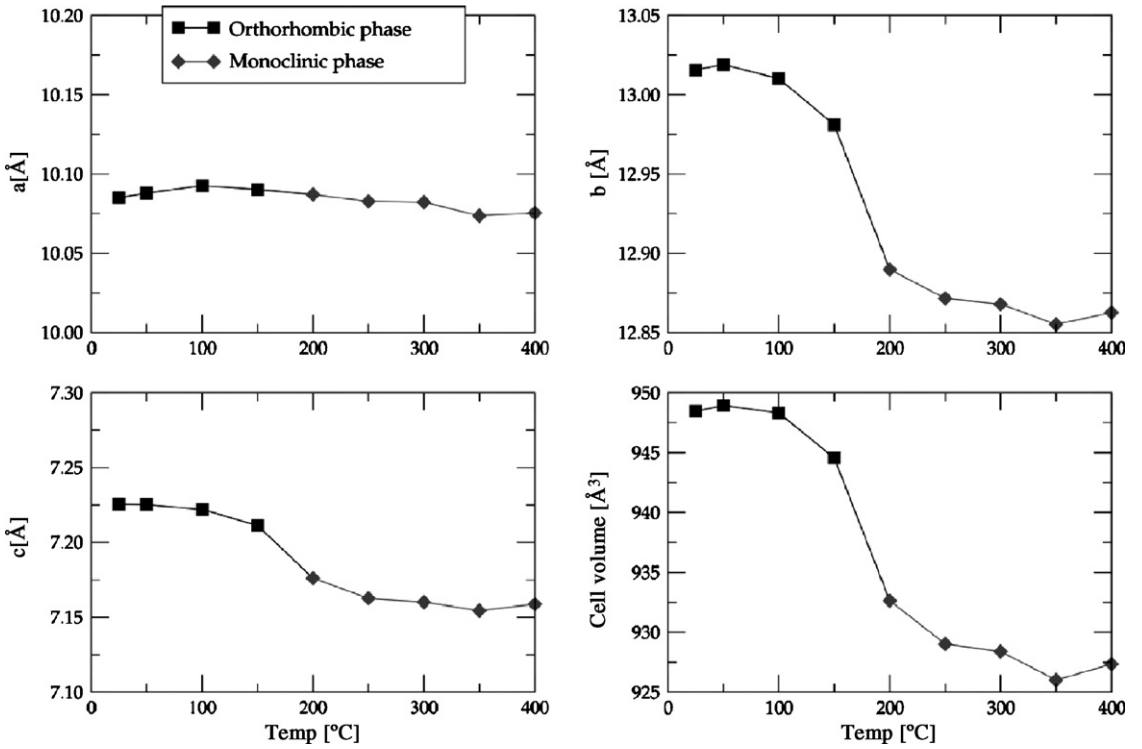

Fig. 6. Changes of cell parameters upon dehydration from 25 to 400 °C. *a* Remains almost constant, but *b*, *c*, and the cell volume decrease mainly between 100 and 250 °C. In this temperature range most of the H_2O is released. Errors for cell dimensions are smaller than the size of the symbols. Cell parameters are also listed in Table 3.

amorphous. Heating to 750 °C leads to crystallisation of several phases (Fig. 7), one of which being a wadeite-type structure of composition $K_xRb_{2-x}TiSi_3O_9$, other phases could not be identified from powder X-ray diffraction patterns. This phase transformation is irreversible and was already observed for $K_2TiSi_3O_9$ [7]. Peak positions of the diffraction pattern collected at room temperature are given in Table 5.

Table 2
Overview of unit cells described in this chapter

Composition	*T* (°C)	*a* (Å)	*b* (Å)	*c* (Å)	*β* (°)	Volume (Å^3)
$K_2TiSi_3O_9{\cdot}H_2O$[a]	25	9.941(1)	12.946(1)	7.1543(7)	90	920.7(2)
$K_{0.18}Rb_{1.82}TiSi_3O_9{\cdot}H_2O$	25	10.0851(2)	13.0157(2)	7.2255(1)	90	948.45(3)
$K_xRb_{2-x}TiSi_3O_9{\cdot}H_2O$[b]	25	10.008(1)	13.012(1)	7.2116(6)	90	939.1(2)
$K_{0.18}Rb_{1.82}TiSi_3O_9{\cdot}H_2O$	50	10.0880(2)	13.0190(2)	7.2253(1)	90	948.93(3)
$K_{0.18}Rb_{1.82}TiSi_3O_9{\cdot}H_2O$	100	10.0926(2)	13.0103(2)	7.2220(1)	90	948.31(3)
$K_{0.18}Rb_{1.82}TiSi_3O_9{\cdot}H_2O$	150	10.0903(2)	12.9810(2)	7.2113(1)	90	944.55(3)
$K_{0.18}Rb_{1.82}TiSi_3O_9$	200	10.0871(3)	12.8898(3)	7.1762(2)	91.709(2)	932.64(4)
$K_{0.18}Rb_{1.82}TiSi_3O_9$	250	10.0828(3)	12.8716(4)	7.1627(2)	91.981(2)	929.03(5)
$K_{0.18}Rb_{1.82}TiSi_3O_9$	300	10.0823(3)	12.8679(3)	7.1602(2)	91.968(1)	928.40(4)
$K_{0.18}Rb_{1.82}TiSi_3O_9$	350	10.0737(2)	12.8552(3)	7.1545(2)	91.873(1)	926.01(4)
$K_{0.18}Rb_{1.82}TiSi_3O_9$	400	10.0755(2)	12.8625(2)	7.1587(1)	91.754(1)	927.30(3)
$K_{0.18}Rb_{1.82}TiSi_3O_9{\cdot}H_2O$	25[c]	10.0623(2)	13.0085(2)	7.2131(1)	90	944.16(3)
$K_xRb_{2-x}TiSi_3O_9$[d]	750	6.6599(5)	10.1397(7)	389.49(5)		
$K_xRb_{2-x}TiSi_3O_9$[d]	25[c]	6.5850(3)	10.0792(5)	378.50(3)		

[a] [9].
[b] Minor phase.
[c] After heating cycle.
[d] Wadeite ($P6_3/m$).

Table 3
Atomic coordinates, site occupancies and displacement parameters for dehydrated Rb-exchanged AM-2 at 400 °C (monoclinic, $P2_1$)

Atom	*x/a*	*y/b*	*z/c*	Occupancy	B_{eq}
Tia	0.0673(4)	0.3110(3)	−0.0111(6)	1	1.02(8)
Tib	0.5455(4)	0.2415(3)	0.5058(6)	1	1.02(8)
Rb1a	0.435(1)	0.625(1)	−0.005(2)	1.00(2)	4.2(2)
Rb1b	0.951(1)	0.938(2)	0.498(2)	0.88(2)	4.2(2)
Rb2a	0.202(1)	0.163(1)	0.443(2)	0.924(9)	4.2(2)
Rb2b	0.732(3)	0.430(3)	0.868(7)	0.30(3)	4.2(2)
Rb3a	0.710(2)	0.416(1)	−0.005(3)	0.70(3)	4.2(2)
Si1a	0.0415(6)	0.5773(4)	0.0035(7)	1	1.02(8)
Si1b	0.5499(5)	0.9794(4)	0.5003(8)	1	1.02(8)
Si2a	0.3751(6)	0.3659(4)	0.1806(7)	1	1.02(8)
Si2b	0.8441(5)	0.2184(4)	0.2848(7)	1	1.02(8)
Si3a	0.3506(5)	0.3587(4)	0.7838(7)	1	1.02(8)
Si3b	0.8418(5)	0.2047(4)	0.6990(8)	1	1.02(8)
Ola	0.223(2)	0.327(4)	0.159(2)	1	1.02(8)
Olb	0.690(2)	0.242(4)	0.329(3)	1	1.02(8)
O2a	0.436(2)	0.382(3)	−0.0243(7)	1	1.02(8)
O2b	0.896(2)	0.183(3)	0.4920(8)	1	1.02(8)
O3a	0.202(2)	0.310(3)	0.798(3)	1	1.02(8)
O3b	0.685(1)	0.231(3)	0.703(2)	1	1.02(8)
O4a	0.138(2)	0.613(1)	0.838(3)	1	1.02(8)
O4b	0.630(3)	0.974(1)	0.702(2)	1	1.02(8)
O5a	0.946(2)	0.293(1)	0.772(2)	1	1.02(8)
O5b	0.412(4)	0.2513(7)	0.699(5)	1	1.02(8)
O6a	0.9165(9)	0.6584(5)	−0.015(6)	1	1.02(8)
O6b	0.430(1)	0.8941(4)	0.495(7)	1	1.02(8)
O7a	0.108(4)	0.5949(8)	0.212(2)	1	1.02(8)
O7b	0.677(1)	0.943(2)	0.383(3)	1	1.02(8)
O8a	0.940(4)	0.305(1)	0.191(5)	1	1.02(8)
O8b	0.411(2)	0.263(1)	0.305(3)	1	1.02(8)
O9a	0.003(1)	0.4549(4)	−0.005(5)	1	1.02(8)
O9b	0.498(2)	0.0960(4)	0.454(4)	1	1.02(8)

Table 4
Atomic coordinates, site occupancies and displacement parameters for fully hydrated Rb-exchanged AM-2 at 25 °C (orthorhombic, $P2_12_12_1$)

Atom	*x/a*	*y/b*	*z/c*	Occupancy	B_{eq}
Ti	0.0545(4)	0.2848(3)	0.7442(6)	1	0.28(7)
Rb1	0.4355(3)	0.5827(2)	0.7694(6)	0.99(1)	2.9(2)
K1	0.4355(3)	0.5827(2)	0.7694(6)	0.01(1)	2.9(2)
Rb2	0.2034(4)	0.1308(3)	0.3105(5)	0.83(1)	2.9(2)
K2	0.2034(4)	0.1308(3)	0.3105(5)	0.17(1)	2.9(2)
Si1	0.0416(5)	0.5485(4)	0.7538(9)	1	0.28(7)
Si2	0.3331(5)	0.3231(4)	0.9707(7)	1	0.28(7)
Si3	0.3525(6)	0.3251(5)	0.5656(7)	1	0.28(7)
O1	0.1765(8)	0.297(1)	0.956(1)	1	0.28(7)
O2	0.405(1)	0.344(1)	0.7741(8)	1	0.28(7)
O3	0.1939(7)	0.309(2)	0.561(1)	1	0.28(7)
O4	0.154(1)	0.5736(9)	0.599(2)	1	0.28(7)
O5	0.948(2)	0.264(1)	0.519(2)	1	0.28(7)
O6	0.9256(9)	0.6336(5)	0.741(3)	1	0.28(7)
O7	0.115(1)	0.5702(8)	0.950(1)	1	0.28(7)
O8	0.907(1)	0.2704(9)	0.921(2)	1	0.28(7)
O9	0.004(1)	0.4294(4)	0.719(3)	1	0.28(7)
Ow1	0.197(2)	0.936(2)	0.405(2)	1	2.9(2)

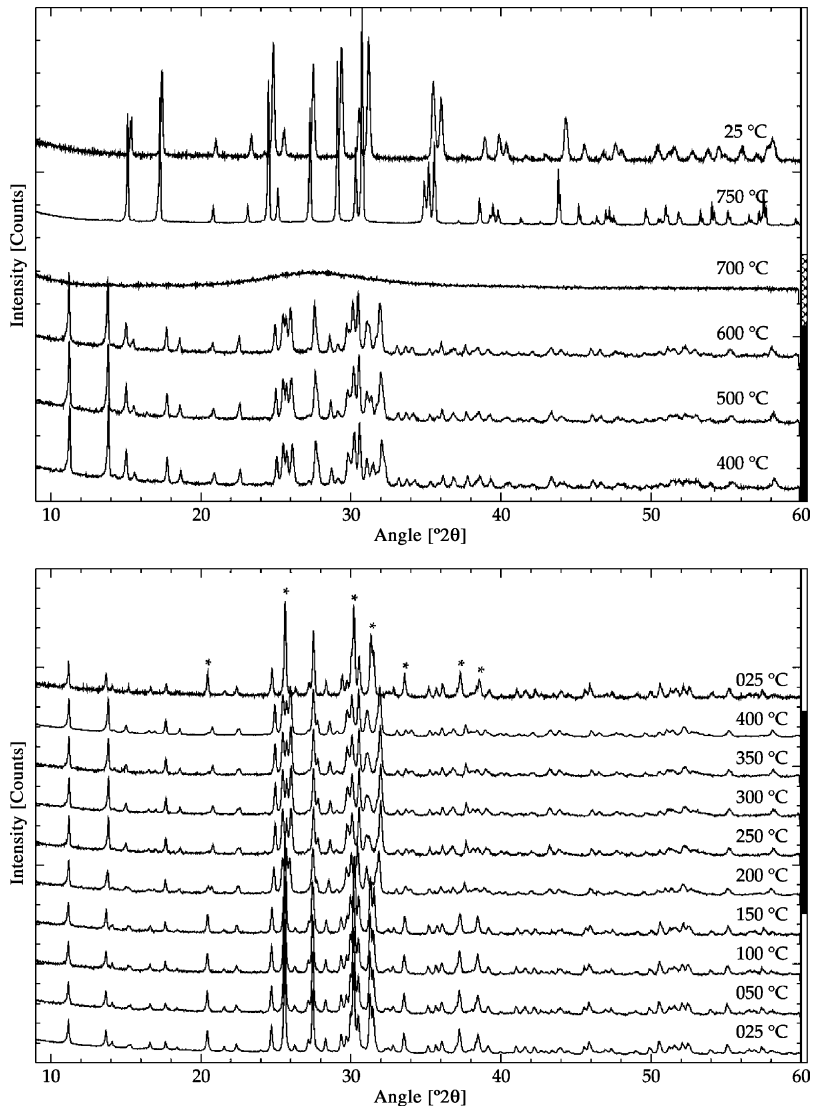

Fig. 7. Bottom: dehydration of Rb-exchanged AM-2 monitored by powder X-ray diffraction shows a distinct phase change between 150 and 200 °C which is completely reversible immediately after room temperature has been reached again. The monoclinic phase is marked with a black bar on the right, whereas the white bar marks the orthorhombic phase. Regions with obvious differences between the two phases are marked with asterisks. Top: the AM-2 structure breaks down between 600 and 700 °C, and a wadeite-type phase crystallises between 700 and 750 °C, which remains stable at room temperature.

4. Discussion

Although the weight loss from 25 to 400 °C monitored by TG analysis corresponds to $1.2H_2O$ molecules pfu, only one ordered H_2O site was found in the structure refinement. This leads to the assumption that probably additional H_2O is adsorbed on the crystal surface. The exchange process plotted in Fig. 4 shows an exponential character and indicates that >99% ion-exchange could have been reached with only one or two more exchange cycles. Even higher selectivity for Rb^+ of AM-2 structures with Zr/Ti ratios > 0.5 have been reported [3], whereas for ratios <0.5 a higher preference for K^+ was observed. Since we reached almost complete exchange with the pure Ti endmember, it is not clear whether the chemical composition or crystal morphology leads to different exchange kinetics.

The cation site Rb1 is located almost exactly at the centre of an eight-membered ring made from six tetrahedra and two octahedra (Fig. 8). It bonds to eight framework oxygens with bonding distances between 2.85(1) and 3.31(2) Å,

Table 5
Peak positions of the diffraction pattern collected at room temperature after heating to 750 °C

2θ	d (Å)	Abs. intensities (cts)	Reflection intensities (%)	$h\,k\,l_{\text{wadeite}}$
15.348	5.768	1538	28	(0 1 0)
17.404	5.091	3064	72	(0 0 2)
20.996	4.228	938	12	
23.360	3.805	1031	15	(0 1 2)
24.236	3.669	588	3	
24.829	3.583	3906	96	
25.539	3.485	1242	21	
27.501	3.241	3290	79	
29.381	3.037	3790	94	
30.560	2.923	1950	42	(0 1 3)
31.186	2.866	4002	100	(0 2 0)
35.496	2.527	2634	62	(0 0 4)
36.021	2.491	2171	49	(0 2 2)
37.459	2.399	516	3	
38.936	2.311	1021	17	(0 1 4)
39.888	2.258	1077	19	
40.372	2.232	863	14	
41.677	2.165	494	3	
42.997	2.102	515	4	
44.339	2.041	1509	32	
45.590	1.988	760	11	
46.844	1.938	566	6	
47.639	1.907	815	13	
48.049	1.892	621	7	
50.397	1.809	768	12	
50.471	1.807	709	10	
50.546	1.804	709	10	
51.209	1.782	601	7	
51.581	1.770	759	11	
52.826	1.732	568	6	
53.748	1.704	647	8	
53.870	1.700	604	7	
54.507	1.682	724	10	
54.933	1.670	520	5	
55.952	1.642	636	8	
56.051	1.639	668	9	
57.065	1.613	536	5	
57.732	1.596	740	11	
58.105	1.586	987	18	

h k l indices of some strong reflections belonging to the wadeite-type structure are given in the fifth column. Other phases are unknown.

seven of which belong to ring-building polyhedra. Bond eight is almost perpendicular to the ring plane fixing Rb1 in three dimensions. Towards the main channel Rb1 bonds to the H_2O site Ow1 with a bond length of 2.93(2) Å. The second channel occupant Rb2 is located at the intersection of the main channel with the interconnecting channel, the latter joining the main channel in a seven-membered ring. At this location the framework leaves relatively large void areas, allowing Rb2 to reside above the ring plane in almost ideal bonding distance to the ring-forming polyhedra. Towards the centre of the main channel it bonds to two H_2O sites, on the opposing side it bonds to five framework oxygens of the seven-membered ring with bond lengths between 2.94(1) and 3.13(1) Å.

Bond valence calculations [13] for all framework atoms show low values to the vertices of the TiO_6 octahedron, which are thus the preferred bonding counterparts for exchangeable cations. The AM-2 structure allows cations to take positions in bonding distance to the framework regularly distributed around TiO_6 octahedra in a rectangular arrangement. This configuration minimises repulsive forces between channel occupants, and since they are located off-centre in the main channels, the pore system remains open and allows cations and H_2O molecules to diffuse in the crystal.

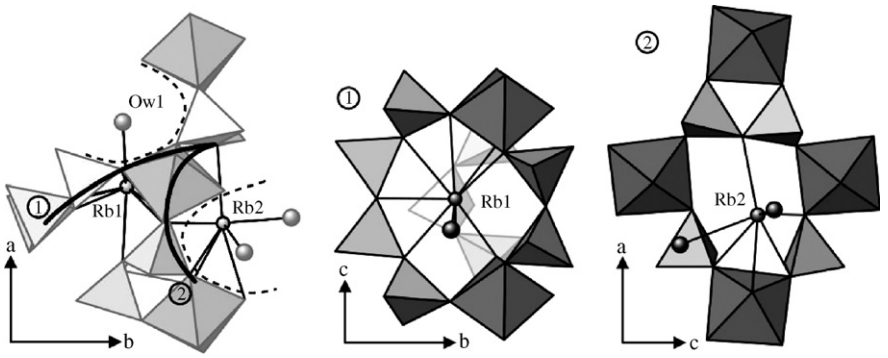

Fig. 8. In the fully hydrated phase the cation position Rb1 is located in the centre of a eight-membered ring (1), whereas Rb2 resides at the intersection of the main channel and an interconnecting channel, the latter joining the main channel in a seven-membered ring (2) in the side wall. The projected planes of the two rings are shown as bold lines in the left figure, main channels are indicated by broken lines. The centre and right figure show the two rings projected roughly perpendicular to the ring planes.

The minor second phase observed in the hydrated diffraction pattern gradually disappeared with increasing temperature and was no longer observed in the dehydrated and re-hydrated phases. We assume that this minor phase represents cores with incomplete ion-exchange. Despite the change to monoclinic symmetry the framework of the dehydrated structure shows only minor changes compared to the orthorhombic variant (Fig. 1). The loss of symmetry operators leads to slightly less regular channel cross-sections, but the framework topology remains unchanged. The sites Rb1a and Rb1b located in the centre of the eight-membered rings remain at their position in bonding distance to two octahedra. They bond to five (Rb1a) and four (Rb1b) vertices of ring-polyhedra, and to three vertices lying outside

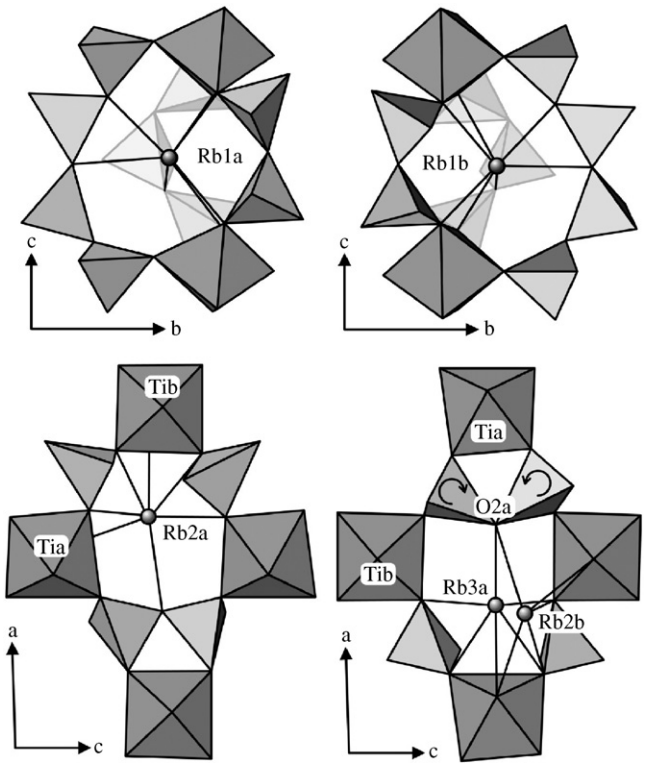

Fig. 9. The bonding situations of Rb cations in dehydrated AM-2. Top: Rb1a/b maintain their positions in the centre of the eight-membered ring. The ring becomes slightly irregular, and both cation positions lose one bond to the framework. Bottom: Rb2a remains almost unchanged, but the stronger bonds of Rb2b and Rb3a to the framework oxygen O2a lead to a rotation of the two connected tetrahedra. This also induces a distortion of octahedron Tia, which becomes trapezoid in cross-section.

of the ring plane (Fig. 9). As in the hydrated structure the sites are strongly fixed in three dimensions. Rb2a also remains at its initial position at the intersection of the main channel and the interconnections. It bonds to seven framework oxygens, six of which being vertices of octahedra. On the splitted position, Rb3a maintains its position at the centre of the seven-membered ring, slightly shifted out of the ring plane towards the centre of the main channel. It bonds to five octahedral vertices and to O2a. The second position Rb2b is more off-centre from the seven-membered ring and bonds four times to octahedra, and also to O2a. Framework oxygen O2a is pulled towards the centre of the seven-membered ring (Fig. 9). This causes the O2a-sharing tetrahedra to rotate and to distort the connected octahedron Tia, which becomes slightly trapezoid in cross-section. The angle of the shifted vertices O1(a)–Ti(a)–O3(a) changes from 93.7(7)° in the orthorhombic phase, to 83(1)° in the monoclinic phase. In addition, units composed of one octahedron and two tetrahedra rotate slightly around [0 1 0] and cause the monoclinic angle to increase above 90°. Distances of Rb sites to framework oxygens are listed in Table 6.

The wadeite structure ($K_xRb_{2-x}TiSi_3O_9$) that crystallises from the amorphous phase above 700 °C is a hexagonal ring-silicate which completely immobilises Rb ions by incorporating them into the silicate framework. In addition, one or more other phases form in quantities comparable to the wadeite phase. We were not able to identify these materials by X-ray diffraction.

Table 6
Rb–O distances <3.37 Å in the hydrated orthorhombic (25 °C, $P2_12_12_1$) and the dehydrated monoclinic (400 °C, $P2_1$) Rb-exchanged AM-2 structure

25 °C		400 °C	
Atom 1–atom 2	Distance (Å)	Atom 1–atom 2	Distance (Å)
Rb1–O1	2.98(1)	Rb1a–Olb	3.00(3)
Rb1–O2	3.13(1)	Rb1a–O2a	3.13(4)
Rb1–O3	2.85(1)	Rb1a–O3b	2.86(3)
Rb1–O4	3.10(1)	Rb1a–O4a	3.16(2)
Rb1–O4	3.26(1)	Rb1a–O4b	3.00(2)
Rb1–O5	2.94(1)	Rb1a–O5b	3.10(3)
Rb1–O7	3.09(1)	Rb1a–O8b	3.22(2)
Rb1–O9	3.31(2)	Rb1a–O9b	3.32(3)
Rb1–Ow1	2.93(2)		
		Rb1b–Ola	3.37(3)
		Rb1b–O2b	3.21(4)
		Rb1b–O3a	3.06(3)
		Rb1b–O5a	2.90(2)
		Rb1b–O7a	2.97(2)
		Rb1b–O7b	2.85(2)
		Rb1b–O8a	2.98(4)
Rb2–O1	3.37(2)	Rb2a–Ola	2.94(4)
Rb2–O2	3.09(1)	Rb2a–O2b	3.13(2)
Rb2–O3	2.95(2)	Rb2a–O3a	3.17(3)
Rb2–O5	3.08(2)	Rb2a–O5b	2.98(4)
Rb2–O8	2.94(1)	Rb2a–O6a	3.26(4)
Rb2–O9	3.13(1)	Rb2a–O8b	2.68(2)
Rb2–Ow1	2.63(2)	Rb2a–O9b	3.10(2)
Rb2–Ow1	3.22(2)		
		Rb2b–Rb3a	0.96(5)
		Rb2b–O2a	3.16(4)
		Rb2b–O3b	2.85(5)
		Rb2b–O5a	2.89(4)
		Rb2b–O6b	3.06(6)
		Rb2b–O9a	2.87(4)
		Rb3a–Olb	3.28(4)
		Rb3a–O2a	2.80(2)
		Rb3a–O3b	3.18(4}
		Rb3a–O5a	3.31(3)
		Rb3a–O8a	3.03(4)
		Rb3a–O9a	2.99(2)

A transformation from orthorhombic to monoclinic symmetry similar to the one we observed between 150 and 200 °C was described for dehydrated AM-2 with Sn in octahedral co-ordination ($K_2SnSi_3O_9{\cdot}H_2O$) [6] and for AM-2 of composition $K_2TiSi_3O_9{\cdot}H_2O$ [14]. As in our Rb-exchanged sample, the transformation of Sn-bearing AM-2 occurred between 150 and 200 °C, but dehydration was faster and subsided at 200° C. These authors suggest that the flexibility of the AM-2 structure is not only decisive for its cation-exchange capacity, but also prevents the crystal structure from breaking down upon loss of H_2O. Structure refinement of dehydrated $K_2SnSi_3O_9{\cdot}H_2O$ was not attempted [6]. A more rigid kostylevite-type polymorph of composition $K_2PbSi_3O_9{\cdot}H_2O$, which is structurally closely related to AM-2, was not able to withstand the dehydration and gradually lost its crystallinity upon dehydration. Ti-AM-2 described in [14] reaches complete dehydration at 360 °C and transforms to monoclinic $P2_1$ between 250 and 300 °C.

From detailed analysis of the Rb-exchanged structure we conclude that the framework topology of hydrated AM-2 provides an excellent bonding environment for two Rb cations. The dehydrated structure provides a similar environment with minor distortions. All exchangeable positions are located off-centre in the main channel, leaving enough space for migration of cations and H_2O molecules through the channel system. In contrast to our clearly orthorhombic hydrated phase $K_{0.18}Rb_{1.82}TiSi_3O_9{\cdot}H_2O$ and also $K_2TiSi_3O_9{\cdot}H_2O$ [9], the structure of umbite, a natural mineral with AM-2 structure and the composition $K_2(Zr_{0.86}Ti_{0.14})Si_3O_9{\cdot}H_2O$, was described as monoclinic, but close to orthorhombic with a unique c axis and $\gamma = 90.07°$ [5]. Although we cannot confirm this symmetry for pure Ti-AM-2 with Rb channel occupants, we observed flexibility of the framework which allows the structure to transform between orthorhombic and monoclinic symmetry without losing its integrity. This flexibility seems to be preserved over a wide range of chemical compositions of the framework structure.

Acknowledgement

This study was supported by the ‘Swiss National Science Foundation’, credit 20-65084.01 to T. Armbruster.

References

[1] M. Nyman, T.M. Nenoff, T.J. Headley, Sandia Report SAND2001-0999, Sandia National Laboratories, Albuquerque, New Mexico 87185 and Livermore, California 94550, 2001.
[2] J. Rocha, M.W. Anderson, Eur. J. Inorg. Chem. 2000 (2000) 801–818.
[3] A. Clearfield, A.I. Bortun, L.N. Bortun, D.M. Poojary, S.A. Khainakov, J. Mol. Struct. 470 (1998) 207–213.
[4] Z. Lin, J. Rocha, P. Brandão, A. Ferreira, A.P. Esculcas, J.D.P. de Jesus, A. Philippou, M.W. Anderson, J. Phys. Chem. B 101 (1997) 7114–7120.
[5] G.D. Ilyushin, Inorg. Mater. 29 (1993) 1128–1133.
[6] P. Pertierra, M.A. Salvadó, S. García-Granda, S.A. Khainakov, J.R. García, Thermochim. Acta 423 (2004) 113–119.
[7] A.I. Bortun, L.N. Bortun, D.M. Poojary, O. Xiang, A. Clearfield, Chem. Mater. 12 (2000) 294–305.
[8] S.R. Jale, A. Ojo, R.R. Fitch, Chem. Commun. 5 (1999) 411–412.
[9] X. Zou, M.S. Dadachov, Acta Crystallogr. Sec. C 56 (2000) 738–739.
[10] K.E. Christensen, X. Zou, personal communication, 2004.
[11] J. Rodríguez-Carvajal, FullProf 2000. Computer program. Version 3.20, 2005.
[12] Z. Lin, J. Rocha, P. Ferreira, A. Thursfield, A.J. Agger, M.W. Anderson, J. Phys. Chem. B 103 (1999) 957–963.
[13] N.E. Brese, M. O’Keeffe, Acta Crystallogr. B47 (1991) 192–197.
[14] N. Döbelin, Microporous titanosilicate AM-2: Synthesis, ion-exchange and dehydration, Ph.D. Thesis, Universitat Bern, 2005, 85 pp.